Cosmogenic ^{3}He dating of alluvial surfaces using detrital magnetite enabled by microCT scanning

SCEC Award # 20146

Final Report

Kenneth Farley[1], Emily Cooperdock[2], Josh West[2], Florian Hofmann[1]
(1) California Institute of Technology, (2) University of Southern California

Abstract

We have tested whether X-ray micro computed tomography (microCT) scanning can improve the quality of cosmogenic magnetite ^{3}He data by pre-selecting mineral grains without inclusions. We extracted magnetite from a paleosol of an offset fanglomerate in the San Gorgonio Pass Special Fault Study Area. We show that inclusions in magnetite can lead to a significant overestimation of the ^{3}He concentration and therefore the exposure age. Grains without inclusions have ^{3}He concentrations close to an expected exponential depth profile after accounting for ^{3}He derived from nucleogenic and cosmogenic neutron produced sources. By comparing the results to an existing depth profile of ^{10}Be and ^{26}Al concentrations in quartz, we calibrate a cosmogenic ^{3}He production rate in magnetite. The method described here, together with the production rate calibration, will make it possible to use ^{3}He in magnetite as a robust tool for cosmogenic exposure studies, adding to the toolkit for quantifying rates of fault motion and other active tectonic processes.

Technical Report

Quantitative estimates of fault slip rates are integral primary data for all subsequent interpretation to understand fault behavior and are a critical SCEC priority. Reliable slip rates can only be obtained if the age determination for offset features is robust. We present a methodology that improves the reliability of cosmogenic ^{3}He exposure dating of magnetite and apply it to a soil on an offset fanglomerate terrace at Whitewater (Owen et al., 2014; Kendrick et al., 2015; Fosdick and Blisniuk, 2018) in the SCEC San Gorgonio Pass Special Fault Study area.

Magnetite (Fe_3O_4) is a common phase in igneous and metamorphic rocks (Buddington and Lindsley, 1964; Nadoll et al., 2012; 2014). It is very retentive to helium (Blackburn et al., 2007) and resistant to weathering. Magnetite can survive transport during erosion either within clasts or as discrete grains in sedimentary sequences, and it can be easily isolated from bulk material. This makes magnetite a potential target phase for cosmogenic ^{3}He exposure dating with wide-spread applicability for dating alluvial surfaces.

However, magnetite frequently has solid and fluid inclusions, which might increase the measured ^{3}He concentration above that of the expected cosmogenic production in magnetite. Magnetite is an opaque phase, therefore inclusions cannot be detected by light microscopy as is the commonly done for transparent phases, such as olivine (e.g. Trull et al., 1991). We scanned magnetite grains using X-ray micro computed tomography (microCT) to investigate the internal structure and identify grains with and without inclusions (Fig. 3). This approach was successfully used by Cooperdock and Stockli (2016) and

Cooperdock et al. (2020) for selecting magnetite crystals for (U-Th)/He thermochronology to avoid the interference caused by other ^{4}He-bearing mineral inclusions.

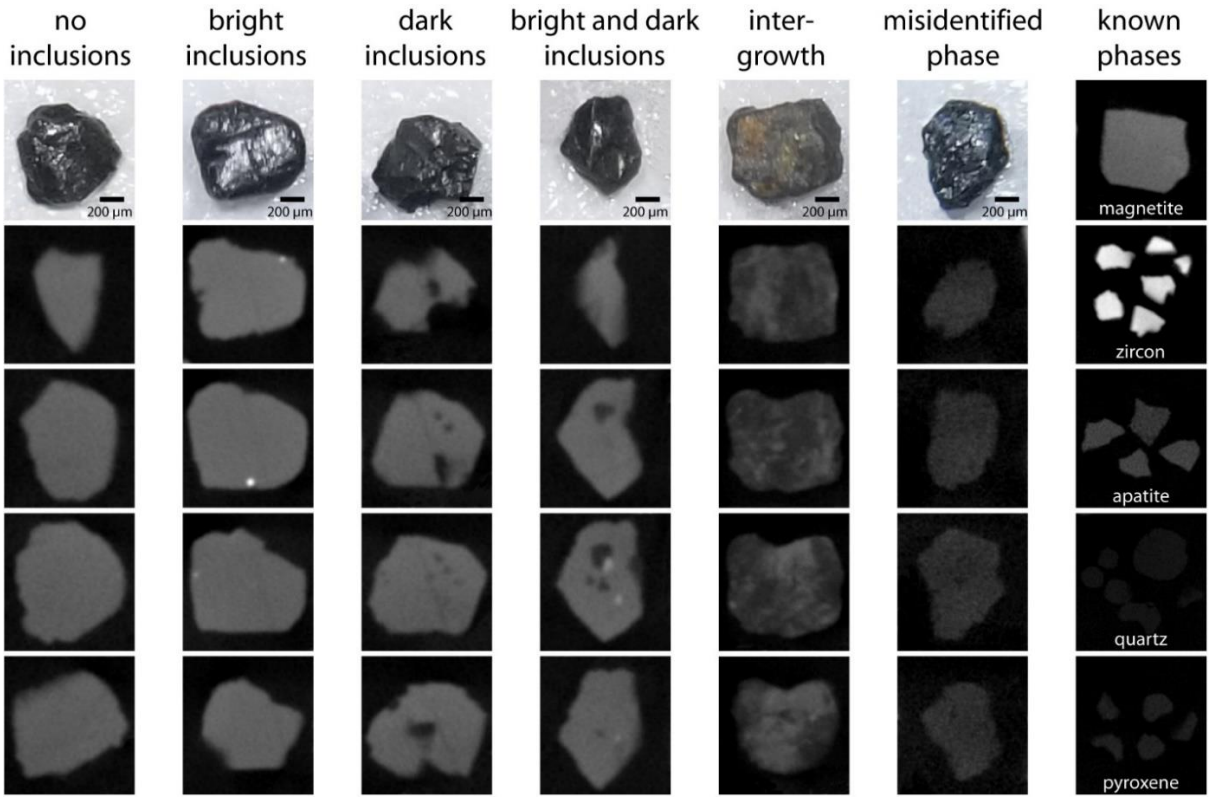

Figure 1: Examples of different types of structures and inclusions in magnetite grains detected with microCT. Light micrographs and four horizontal slices of microCT images are given. All microCT data was acquired with the same scan parameters and images are given at the same contrast. Reference microCT images for known phases are given for comparison. Bright inclusions represent zircon and apatite, whereas inclusions darker than magnetite are most likely silicates. Intergrowth/substitution structures and other phases mistakenly identified as magnetite during sample picking under a light microscope were also detected.

Based on the microCT analysis. we selected aliquots of magnetite grains with and without inclusions and measured ^{3}He concentrations on a depth profile (Fig. 2). Aliquots without inclusions are close to the expected cosmogenic depth profile based on independent ^{10}Be chronology. In contrast, grains with inclusions and magnetite grains picked without information about the internal structure show elevated ^{3}He and ^{4}He concentrations. These data show that inclusions can create excess ^{3}He concentrations up to a factor of four above the cosmogenic production. If aliquots with inclusions were used for calculating exposure ages, they would be vastly overestimated relative to the true exposure age. Our results highlight the need to exclude inclusion when measuring ^{3}He concentrations for cosmogenic exposure studies.

We measured Li concentrations, major and trace element compositions, and (U-Th)/He cooling ages of magnetite in order to model the non-cosmogenic production of ^{3}He. Measured ^{3}He concentrations were corrected for the nucleogenic, cosmogenic thermal neutron, and radiogenic components of ^{3}He

production. The depth profile of these corrected concentrations (Fig. 3) was used to calibrate the ^{3}He production rate in magnetite by comparing it to an existing depth profile of ^{10}Be and ^{26}Al in quartz taken from the same sample material (Hofmann, 2019). With a known exposure age of 53.5 ka, which is with error of the age determined by a previous study (Owen et al., 2014), a best-fit model yielded a local production of 158±18 at/g/a (2σ). This local production rate was scaled to sea-level and high latitude (SLHL) using a time-constant scaling factor of 1.358 (Lal, 1991). The SLHL ^{3}He production rate determined for the Whitewater site is 116±13 at/g/a (2σ).

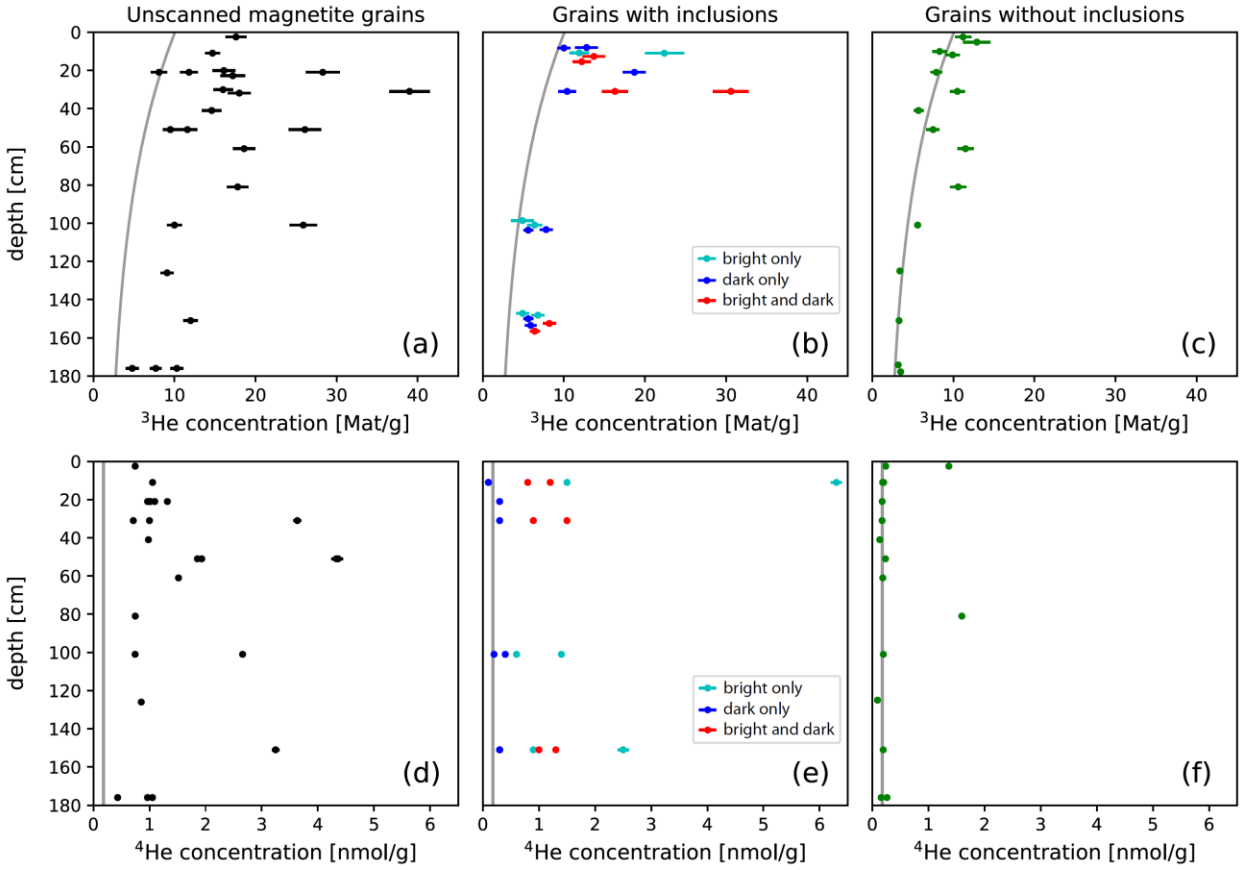

Figure 2: Depth profiles of measured ^{3}He (top row) and ^{4}He (bottom row) concentrations from unscreened magnetite grains without information about inclusions (black), samples with bright (turquoise), dark (blue), as well as bright and dark inclusions (red), and samples without inclusions (green). All uncertainties shown are at the 1σ level and overlapping data points have been slightly vertically offset for clarity. The expected cosmogenic ^{3}He depth profile based on the known exposure age and the average ^{4}He concentration of aliquots without inclusions are shown as grey lines. Samples without inclusions have ^{3}He concentrations close to the predicted depth profile and all but two have low, nearly constant ^{4}He concentrations (around 0.2 nmol/g). Grains with inclusions have significantly higher ^{3}He and ^{4}He concentrations, showing the effects of radiogenic and thermal neutron produced ^{3}He added by these inclusions. The ^{3}He concentration decreases with depth even in grains with inclusions, indicating a cosmogenic thermal neutron component to nucleogenic production.

Our magnetite SLHL production rate is higher than previous estimates from element-specific production rates of 66 at/g/a (cf. Masarik and Reedy, 1996) and calibrations of 69-77 at/g/a (Bryce and Farley, 2002). It is, however, within uncertainty of the modeled (122 at/g/a) and calibrated (120±12 at/g/a) production rate of Kober et al. (2005) for Fe-Ti-oxides. The production rate determined here will make it possible to calculate exposure ages from ^{3}He concentration in magnetite in the future.

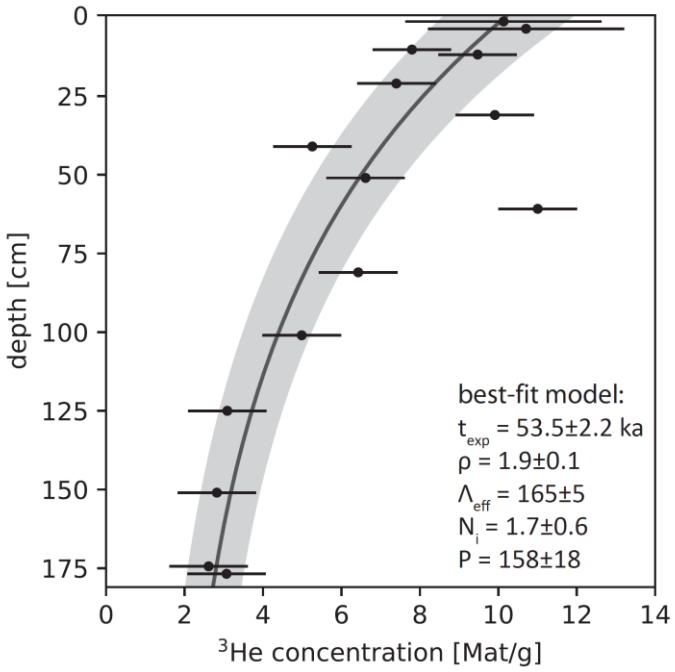

Figure 3: Depth profile of measured ^{3}He concentrations in magnetite without inclusions corrected for nucleogenic and CTN-produced ^{3}He with 2σ uncertainties. Replicate analyses at the same depth are shown with a slight vertical offset for clarity. The solid line and shaded area show the best-fit model with 2σ uncertainty using a known exposure age (t_{exp}), bulk density (ρ), and effective attenuation length (Λ_{eff}). The model was optimized for the inherited concentration (N_i) and the local surface production rate (P).

Mineral inclusions including quartz, feldspar, apatite, and zircon contribute significant amounts of ^{3}He to magnetite grains, which in the samples studied here can lead to an excess of a factor of four above the cosmogenically produced amount of ^{3}He. Contribution of ^{3}He from mineral inclusions can be prevented by screening magnetic separates using microCT and selecting only those grains without inclusions. Knowledge of the U and Li concentration of the magnetite as well as the matrix and the redistribution of ^{3}He due to the kinetic energy of the produced particle, is important to correct measured ^{3}He concentrations for the nucleogenic, cosmogenic thermal neutron, and radiogenic components.

In summary, by screening magnetite separates using microCT to select only inclusion-free grains and accounting for non-cosmogenic production, ^{3}He in magnetite can be used as a robust tool for in-situ and detrital cosmic-ray exposure studies. This technique might also help to improve the quality of cosmogenic ^{3}He measurements of other opaque phases.

Publication

Florian Hofmann, Emily Cooperdock, Joshua West, Dominic Hildebrandt, Kathrin Strößner, Kenneth A. Farley: Exposure dating of detrital magnetite using ^{3}He enabled by microCT and calibration of the cosmogenic ^{3}He production rate in magnetite. In preparation.

References

Bryce J.G., and Farley K.A. (2002): ^{3}He exposure dating of magnetite, in: F.A. Podosek (Ed.), Goldschmidt Conference Abstracts 2002, A108.

Buddington A.F., and Lindsley D.H. (1964): Iron-titanium oxide minerals and synthetic equivalents. Journal of Petrology 5(2), 310-357.

Cooperdock E.H., and Stockli D.F. (2016): Unraveling alteration histories in serpentinites and associated ultramafic rocks with magnetite (U-Th)/He geochronology. Geology 44(11), 967-970.

Cooperdock E.H.G., Stockli D.F., Kelemen P. B., and de Obeso J. C. (2020): Timing of magnetite growth associated with peridotite-hosted carbonate veins in the SE Samail ophiolite, Wadi Fins, Oman. Journal of Geophysical Research: Solid Earth 125(5), e2019JB018632.

Fosdick J. C., and Blisniuk K. (2018): Sedimentary signals of recent faulting along an old strand of the San Andreas Fault, USA. Scientific reports 8(1), 1-10.

Kendrick K.J., Matti J.C., and Mahan S.A. (2015): Late Quaternary slip history of the Mill Creek strand of the San Andreas fault in San Gorgonio Pass, southern California: The role of a subsidiary left-lateral fault in strand switching. Bulletin 127(5-6), 825-849.

Kober F., Ivy-Ochs S., Leya I., Baur H., Magna T., Wieler R., and Kubik P.W. (2005): In situ cosmogenic ^{10}Be and ^{21}Ne in sanidine and in situ cosmogenic ^{3}He in Fe-Ti-oxide minerals. Earth and Planetary Science Letters 236(1-2), 404-418.

Masarik J., and Reedy R.C. (1996): Monte Carlo simulation of in-situ-produced cosmogenic nuclides. Radiocarbon 38(1), 163-164.

Nadoll P., Mauk J.L., Hayes T.S., Koenig A.E., and Box S.E. (2012): Geochemistry of magnetite from hydrothermal ore deposits and host rocks of the Mesoproterozoic Belt Supergroup, United States. Economic Geology 107(6), 1275-1292.

Nadoll P., Angerer T., Mauk J. L., French D., and Walshe J. (2014): The chemistry of hydrothermal magnetite: a review. Ore Geology Reviews 61, 1-32.

Owen LA, Clemmens SJ, Finkel RC, and Gray H (2014): Late Quaternary alluvial fans at the eastern end of the San Bernardino Mountains, Southern California. Quaternary Science Reviews 87, 114-134.

Trull T.W., Kurz M.D., and Jenkins W.J. (1991): Diffusion of cosmogenic ^{3}He in olivine and quartz: implications for surface exposure dating. Earth and Planetary Science Letters 103(1-4), 241-256.